Use of Differentiable and Nondifferentiable Optimization Algorithms for Variational Data Assimilation with Discontinuous Cost Functions

S. Zhang, X. Zou*, J. Ahlquist, I. M. Navon

Florida State University, Tallahassee, Florida, USA

J. G. Sela

National Centers for Environmental Prediction, Maryland, USA

December 1999

(submitted to Mon. Wea. Rev.)

* Corresponding author: Department of Meteorology, Florida State University, 404 Love Bldg., Tallahassee, FL 32306-4520. email: zou@met.fsu.edu. phone: (850) 644-6025.

ABSTRACT

Cost functions formulated in four-dimensional variational data assimilation (4D-Var) are nonsmooth in the presence of discontinuous physical processes (i.e., the presence of "on-off" switches in NWP models). The adjoint model integration produces values of subgradients, instead of gradients, of these cost functions with respect to the model's control variables at discontinuous points. Minimization of these cost functions using conventional differentiable optimization algorithms may encounter difficulties. In this paper we use an idealized discontinuous model and an actual shallow convection parameterization, both including "on-off" switches, to illustrate the performances of differentiable and nondifferentiable optimization algorithms. It was found that (i) the differentiable optimization, such as the limited memory quasi-Newton (L-BFGS) algorithm, may still work well for minimizing a nondifferentiable cost function, especially when the changes made in the forecast model at switching points to the model state are not too large; (ii) for a differentiable optimization algorithm to find the true minimum of a nonsmooth cost function, introducing a local smoothing that removes discontinuities may cause more problems than solutions due to the insertion of artificial stationary points; and (iii) a nondifferentiable optimization algorithm is found to be able to find the true minima in cases where the differentiable minimization failed. For the case of strong smoothing, differentiable minimization performance is much improved, as compared to the weak smoothing cases.

1 Introduction

Since optimal control theory was introduced into atmospheric data assimilation by Le Dimet and Talagrand (1986), four-dimensional variational data assimilation (4D-Var) has been used for atmospheric data assimilation, initially in a research mode, and currently moving toward an operational implementation (Thépaut and Courtier, 1991; Navon et al., 1992; Zupanski and Mesinger, 1995; Kuo et al., 1996; Zou, 1997; Rabier et al., 1998; Zou et al., 1999). The 4D-Var approach adjusts the control variables of a numerical weather prediction (NWP) model to their optimal values by minimizing a specified error measurement called the cost function. Information in observations is extracted, based not only on background and observational error covariances, but also on model dynamical and physical constraints. Due to its sound mathematical basis, 4D-Var is receiving more and more attention in the applications of NWP.

The optimization procedure in 4D-Var is completed by employing a large-scale unconstrained minimization algorithm. Among several choices, the limited memory quasi-Newton algorithm (Broyden-Fletcher-Goldfarb-Shanno, 1970; Liu and Nocedal, 1989; hereafter refereed to L-BFGS) was found to be one of the most efficient when the dimensions of the control variable are large, i.e., the dimensions of the control variables are greater than 10^5 (Zou et al., 1993). The most attractive advantage of the L-BFGS algorithm is its modest storage requirement and good convergence rate (Zou et al., 1993). The algorithm was originally designed for minimizing differentiable cost functions. Early 4D-Var experiments used either simple models or adiabatic primitive equation models without parameterized physics. The cost functions defined by these models are differentiable since solutions of the assimilation model are differentiable and the governing equations are uniformly valid over a global domain. Therefore, the L-BFGS algorithm, which is based on the assumption that the cost function is differentiable, has performed very well (Navon et al., 1992; Zou et al. 1993)

Nonsmooth cost functions, i.e., cost functions with discontinuous gradients, arise in 4D-Var when assimilation models include discontinuous physical processes. A more complex diabatic model including parameterized physics simulates the evolution of the true atmospheric state better than an adiabatic one. Various physical processes are included in the conservation equations of physical variables such as momentum, mass and energy. The physical processes are controlled by local conditions that form a set of "IF" statements depending on model variables and prescribed threshold values. These "IF" statements are often called "on-off" switches since they determine whether a certain physical process should be turned on or off. The presence of "on-off" switches renders the diabatic model solution nondifferentiable, which in turn makes the cost function defined by a diabatic model nondifferentiable even if the cost function itself is a continuous function (usually a quadratic form) of the model solution.

Computational methods of smooth and nonsmooth optimization algorithms were developed that do not assume a specific structure of the minimized function, but require only the evaluation of the function and its gradients (or their analogues in the nondifferentiable case, which are referred to as generalized gradients or subgradients) at any given point. For a class of almost everywhere differentiable functions (such as piecewise differentiable functions), the subgradients are points of nondifferentiability and can be defined by taking limits, or any linear combinations of them with the sum of the coefficients being unity.

Attempts have been made to carry out 4D-Var using a diabatic model to assimilate rainfall observations (Zupanski et al., 1995; Zou and Kuo, 1996; Tsuyuki, 1997) and to improve analysis in tropics (Rabier et al., 1999). There are at least two methods that have dealt with the "on-off" switches in the physical parameterization schemes used in 4D-Var. One consists of introducing a transitional function to make the nonlinear model solution smooth (local smoothing), i.e., carrying out a local smoothing to remove the discontinuities caused by "on-off" switches (Zupanski, 1993; Tsuyuki, 1997). The other keeps the "on-off" switches in the tangent linear and the adjoint models the same as in the nonlinear model (Zou et al., 1993). As discussed in Zhang and Zou (1999), an integration of the adjoint model in which the "on-off" switches are kept the same as in the nonlinear model provides the gradient of the cost function at a differentiable point and a subgradient (the limit of gradients close to the discontinuous point) at a nondifferentiable point. The questions that need to be answered are: (i) Does local smoothing eliminate problems related to "on-off" switches, (ii) does it cause other problems? (iii) What are the potential problems when a differentiable optimization algorithm is employed for minimizing a nondifferentiable cost function?

It is worth mentioning that in practice there is no sharp distinction between nonsmooth and smooth functions. From the point of view of applied mathematics and computational practice, a function with a rapidly changing gradient is similar in its properties to a nonsmooth cost function. Therefore, one may expect that a differentiable optimization algorithm may work well for minimizing a nondifferentiable cost function.

In this paper, a simple model containing a typical form of the discontinuity in an NWP model is used to illustrate the performance of the L-BFGS algorithm with and without removing discontinuities by smooth functions. A nondifferentiable optimization (Lemaréchal, 1978, 1989, 1997) is employed to find the minimum of a cost function for cases when the L-BFGS fails to find the true minimum. Then a physical parameterization scheme (the shallow convection scheme in the NCEP global spectral model) is used to examine the performance of both the differentiable and the nondifferentiable minimization algorithms (Section 3). Conclusions and discussions are presented in section 4.

2 A discontinuous cost function using an idealized simple model with "on-off" switches

2.1 A nonsmooth cost function defined by a discontinuous model

We use an idealized model with a single variable and a typical form of discontinuous physics to examine the behavior of a differentiable minimization to solve nonsmooth problems. The numerical forecast model takes the form of

$$\frac{\partial x}{\partial t} = \begin{cases} f_1(x) & \text{if } x < x_c \\ f_2(x) & \text{if } x \geq x_c \end{cases} \tag{1}$$

where $f_1(x)$ and $f_2(x)$ represent two parameterized physical processes identified by a threshold value x_c.

We can consider a cost function defined as the quadratic form of the model predicted state at time t_R:

$$J_1(x_0) = x^2(t_R) \tag{2}$$

and

$$\frac{\partial x}{\partial t} = \begin{cases} 2x - 2 & as\, x < 1 \\ x - 4 & as\, x \geq 1 \end{cases} \tag{3}$$

where $x_0 = x(t_0)$ and $t_R > t_0$.

The discretization of the forecast model is carried out by using a time step $\Delta t = 0.1$. The length of the assimilation time window is $t_R = t_0 + 4\Delta t$.

2.2 Performance of the L-BFGS algorithm

The performance of the limited-memory quasi-Newton (L-BFGS) method of Liu and Nocedal (1989) is examined with different initial guess values for x_0.

Figure 1 shows that the minimization using the L-BFGS method converged with the initial guess of a) $x_0^{(0)} = 2.00$, b) $x_0^{(0)} = 2.29$, c) $x_0^{(0)} = 2.80$ or d) $x_0^{(0)} = 2.90$. However, the minimization failed to find the true minimum $x_0^* = 0.5$ if it starts with an initial guess of $x_0^{(0)} = 2.55$ (Fig. 2). After about five iterations, the minimization was trapped in a local minimum generated by the "on-off" switches, causing the iterative procedure to switch back and forth between $x_0^{(0)} = 1.521(J = 0.41)$ and $x_0^{(0)} = 1.518(J = 0.99)$.

In order to gain some insight into the general performance of the L-BFGS method, we selected 300 points in the interval $[0, 3]$ for $x_0^{(0)}$, incremented by 0.01 for the successive initial guess points. Numerical results are presented in the second row of Table 1. The L-BFGS minimization failed to find the true minimum in 18 cases. In the other 282 cases, it converged to the true solution.

We found that the total number of minimization failures depends strongly on the size of the jump in the forecast model, and thus the size of the jump in the cost function. When $f_2(x) = x - 4$ is replaced with $f_2(x) = x - 3.5$ (i.e., the size of the jump is reduced), the total number of failing cases was reduced from 18 to 13. If the size of the jump is further reduced, say $f_2(x) = x - 3$, the L-BFGS algorithm successfully finds the solution ($x_0 = 0.5$) for the entire 300 cases tested while increasing the jump size generally leads to more failing cases.

This example suggests that the differentiable minimization may still work well for solving nondifferentiable 4D-Var problems, especially when the sizes of the jumps caused by discontinuous physics are small. However, it is possible that the differentiable minimization may remain stuck with a local minimum and fail to find the true minimum. The possibility of encountering a minimization failure in the presence of a discontinuity is greater when the forecast model contains larger jumps.

2.3 Introducing a local smooth function to remove discontinuities

Given the fact that the presence of discontinuities associated with "on-off" switches in the 4D-Var assimilation model may cause difficulties for the minimization in finding the true minimum, a natural step to remedy this situation is to introduce a smooth transitional function to remove the discontinuities (Zupanski et al., 1995; Tsuyuki, 1997). For example, a function

$$f_{smooth} = 0.5\{1 + \tanh[\alpha(x - x_c)]\} \tag{4}$$

is introduced into the assimilation model at threshold points, where α is a scalar which controls the accuracy of the smoother. The transition is implemented by calculating $f_{transition}$ as

$$f_{transition}(x) = \begin{cases} \frac{f_1(0.9)+f_2(1.1)}{2} + [\frac{f_1(0.9)+f_2(1.1)}{2} - f_1(x)](2f_{smooth} - 1) & \text{if}\, x_c - h \leq x < x_c \\ \frac{f_1(0.9)+f_2(1.1)}{2} - [\frac{f_1(0.9)+f_2(1.1)}{2} - f_2(x)](2f_{smooth} - 1) & \text{if}\, 1 \leq x < x_c + h \end{cases} \tag{5}$$

and define the forecast model after smoothing as

$$\frac{\partial x}{\partial t} = f(x)$$

$$f(x) = \begin{cases} f_1(x) & \text{if}\, x < x_c - h \\ f_{transition}(x) & \text{if}\, x_c - h \leq x < x_c + h \\ f_2(x) & \text{if}\, x \geq x_c + h \end{cases} \tag{6}$$

where h is a small positive scalar. Choosing $h = 0.1$ and $\alpha = 100$ (a weak smoothing), the introduction of the transitional smooth function produces a smooth distribution of the source term $f(x)$ (thick dotted line in Fig. 4), and a continuous distribution of the cost function in the control variable space (dotted line in Fig. 5a). However, the introduction of the smooth function into the forecast model changes the distribution of the gradient of J with respect to the control parameter (Fig. 5b), introducing additional stationary points. The cost function without smoothing has a unique stationary point (zero-gradient) which corresponds to the true solution ($x_0 = 0.5$) (solid line in Fig. 5b), while the one with smoothing has two extra stationary points for each jump (dotted line in Fig. 5b). Therefore, although the gradient may be discontinuous when the "on-off" switches in the adjoint model are kept the same as in the nonlinear model, such a discontinuity in the gradient does not change the general convexity feature, and the adjoint model integration provides useful subgradient information (see section 2.4 and Zhang et al., 2000). However, a smooth function which seems to remove the discontinuity may introduce false stationary points, which may render the minimization to converge to a wrong solution (Zou et al., 1993).

We indicate, however, that when a very strong smoothing is applied (e.g., the value of α is reduced and that of h is increased), the zig-zag behavior of the cost function can be eliminated and the artificial stationary points will not exist. Figure 6 shows the distributions of the smoothed $f(x)$ if $h = 0.2$, $\alpha = 20$ (thick dashed line) and $h = 0.5$, $\alpha = 5$ (thick dotted-dashed line). The resulting cost function and gradient distributions are displayed in Fig. 7a and Fig. 7b (thick dashed line for $h = 0.2$, $\alpha = 20$ and thick dotted-dashed line for $h = 0.5$, $\alpha = 5$), respectively. It is found that with a strong smoothing, the zig-zag behavior of the cost function is eliminated and the minimization of the smoothed cost function using a differentiable optimization algorithm performs well. But the impact of such a strong smoothing on model solutions need to be investigated before it is applied in 4D-Var.

In order to test the performance of the L-BFGS method for the cost function in which the discontinuity is removed by a transitional smooth function, we repeated the experiments carried out in section 2.2 without the local smoothing function introduced at the switch point. Figure 8 displays the performance of the L-BFGS algorithm on the smoothed cost function with the same length of time integration and initial guess points as in Fig. 1. For all four cases examined, the minimization algorithm stuck at a local stationary point, instead of the true minimum.

When all 300 cases are repeated with a weak local smoothing, we find that there are cases for which the minimization with smoothing succeeds and the one without smoothing fails. The introduction of a weak smoothing increases the total number of failed cases, which is not observed in the case of strong smoothing. Table 1 summarizes the performances of the L-BFGS algorithm without smoothing, with a weak smoothing ($h = 0.1$ and $\alpha = 100$), and with a strong smoothing ($h = 0.5$ and $\alpha = 5$). Compared with the results without smoothing, the introduction of a weak smooth function increased the total number of failed cases by a factor of two. For $f_2(x) = x - 3.0$, or $x - 2$, or $x - 1.5$, the introduction of a weak smooth function produces 18 failed cases for the L-BFGS method while the L-BFGS minimization had no problem finding the true minimum without smoothing. These results indicate that the local smoothing for discontinuous physics may sometimes do more damage than good in 4D-Var with discontinuous physics.

Table 1: The performance of the L-BFGS method

$f_2(x)$	Jump size in the model	ratio between the failed and successful cases		
		no smoothing	weak smoothing	strong smooth
x-4.5	3.5	37/300	54/300	0/300
x-4.4	3.4	24/300	54/300	0/300
x-4.3	3.3	28/300	54/300	0/300
x-4.2	3.2	19/300	44/300	0/300
x-4.1	3.1	15/300	52/300	0/300
x-4.0	3.0	18/300	37/300	0/300
x-3.5	2.5	13/300	20/300	0/300
x-3.0	2.0	0/300	18/300	0/300
x-2.0	1.0	0/300	18/300	0/300
x-1.5	0.5	0/300	19/300	0/300

2.4 Performance of the bundle method for nonsmooth cost functions

Most differentiable minimization algorithms depend on two basic assumptions: (i) the negative gradient at a given point is the steepest direction and is used to approximate the search direction; and (ii) the cost function achieves a monotone and significant decrease along the search direction at each iteration. For a convex nonsmooth function, the direction negative to that of a subgradient is not always a direction of descent. The differentiable unconstrained minimization algorithms, such as L-BFGS, can fail in minimizing a nonsmooth cost function, as was shown in section 2 for the L-BFGS method. Nondifferential minimization algorithms, therefore, consider only the basic facts of convex analysis for convex functions, including nondifferential ones. There are various types of nonsmooth optimization algorithms. The basic mathematical considerations related to implementation of nonsmooth optimization are briefly described below.

2.4.1 Bundle methods in nonsmooth optimization

A nondifferentiable minimization algorithm uses subgradients, called generalized gradients instead of gradients, to attempt to force the function to decrease along the subgradient direction. A vector $\boldsymbol{\partial} J(\mathbf{x}) \in \Re^n$ is called the subgradient of $J(\mathbf{x})$ at the point $\mathbf{x}$, if it satisfies

$$J(\mathbf{x}+\mathbf{y}) \geq J(\mathbf{x}) + < \boldsymbol{\partial} J(\mathbf{x}), \mathbf{y} >, \ \forall \mathbf{y} \in \Re^n \tag{7}$$

where $J(\mathbf{x})$ is a convex function in $\Re^n$, which is minimized. The subgradient method generalizes the gradient method and the quasi-Newton method for differentiable functions (Shor, 1985; Kiwiel, 1985; Poljak, 1977).

At the nondifferentiable point, the cost function can be expressed as a selection among "pieces" (see (1) as an example). Then a popular way to construct the subgradient is a linear combination of gradients corresponding to every piece ($\nabla_i J, i \in I(\mathbf{x})$), as

$$\boldsymbol{\partial} J(\mathbf{x}) = \sum_{i \leq I(\mathbf{x})} \alpha_i \nabla_i J(\mathbf{x}),\ \ \alpha_i \geq 0 \text{ and } \sum_{i \leq I(\mathbf{x})} \alpha_i = 1 \tag{8}$$

The subgradient minimization for $J(\mathbf{x})$ on $\Re^n$ is an iterative process of the form

$$\mathbf{x}_{k+1} = \mathbf{x}_k - \gamma_k \boldsymbol{\partial} J(\mathbf{x}_k) / \|\boldsymbol{\partial} J(\mathbf{x}_k)\| \tag{9}$$

where $\gamma_k \geq 0$ is a stepsize.

For a single iterative point $\mathbf{x}_k$, $-\boldsymbol{\partial} J(\mathbf{x}_k)$ still may not be a descent direction. A few further improvements finally form the bundle method. First, the search direction in the basic subgradient method given by:

$$\mathbf{d}^{(k)} = -\boldsymbol{\zeta}_J^{(k)} / \|\boldsymbol{\zeta}_J^{(k)}\| \text{ where } \boldsymbol{\zeta}_J^{(k)} \equiv \boldsymbol{\partial} J(\mathbf{x}_k) \tag{10}$$

is modified by introducing a space-dilation method (Kiwiel, 1985; Shor, 1985) as

$$\mathbf{d}^{(k)} = \frac{-\mathbf{B}^{(k)} \boldsymbol{\zeta}_J^{(k)}}{\left[\boldsymbol{\zeta}_J^{(k)T} \mathbf{B}^{(k)} \boldsymbol{\zeta}_J^{(k)}\right]^{\frac{1}{2}}} \tag{11}$$

where $\mathbf{B}^{(k)}$ is a space-dilation matrix that implements the space transformation on the subgradient to carry out a more efficient descent. Second, the stopping criterion in the line search has to be modified, since an arbitrary subgradient does not yield information about optimality condition. The bundle methods (Lemaréchal, 1977, 1978; Hiriatt-Urraty and Lemaréchal, 1993) exploit the previous subgradient iterations by gathering subgradient information into a bundle to approximate the whole subdifferential $\boldsymbol{\partial} J(\mathbf{x}^{(k)})$.

It is assumed that, in addition to current iteration point $\mathbf{x}^{(k)}$, there exist auxiliary points $\mathbf{y}^{(j)} \in \Re^n$ from past iterations and subgradients

$$\boldsymbol{\zeta}_J^{(j)} \in \boldsymbol{\partial} J(\mathbf{y}^{(j)})\ j \in I_J^{(k)} \tag{12}$$

where the index-set $I_J^{(k)}$ is a non-empty subset of $\{1, 2, \ldots, k\}$. The search direction in the bundle algorithm is obtained as a solution of the quadratic optimization problem

$$\min_{\mathbf{d},v}(\frac{1}{2}u^{(k)}\mathbf{d}^T\mathbf{d} + v) \tag{13}$$

subject to $-\alpha_J(\mathbf{x}^{(k)}, \mathbf{y}^{(j)}) + (\boldsymbol{\zeta}_J^{(j)})^T\mathbf{d} \leq v \; (j \in I_J^{(k)})$ where $u^{(k)} > 0$ is some weighting parameter and v is a constant term (scalar) in the quadratic form, and

$$\alpha_J(\mathbf{x}^{(\mathbf{x})}, \mathbf{y}^{(j)}) = J(\mathbf{x}^{(k)}) - J(\mathbf{y}^{(j)}) - (\boldsymbol{\zeta}_J^{(j)})^T(\mathbf{x}^{(k)} - \mathbf{y}^{(j)})$$

denotes the linearization error at $\mathbf{x}^{(k)}$.

The next bundle iteration point is obtained via the following line-search strategy:

Let $\mathbf{y}^{(k+1)} = \mathbf{x}^{(k)} + \lambda^{(k)}\mathbf{d}^{(k)}$ for some $\lambda^{(k)} > 0$.

Let $\boldsymbol{\zeta}_J^{(k+1)} \in \boldsymbol{\partial} J(\mathbf{y}^{(k+1)})$

Then if $J(\mathbf{y}^{(k+1)}) \leq J(\mathbf{x}^{(k)}) - \delta^{(k)}$ for some $\delta^{(k)} > 0$,

(i) make a serious step $\mathbf{x}^{(k+1)} = \mathbf{y}^{(k+1)}$,

(ii) otherwise, make a null-step $\mathbf{x}^{(k+1)} = \mathbf{x}^{(k)}$.

In both cases add $\boldsymbol{\zeta}_J^{(k+1)}$ to the existing bundle.

2.4.2 Numerical results

We choose to use the bundle method of Lemaréchal (1977, 1978) and compare its performance with that of the L-BFGS method. The subgradients (or subdifferentials), instead of gradients, are used in this method at nondifferentiable points. From (8), we know that this method using subgradient takes smoothing on gradient rather than the function itself in order to seek a decrease direction. The advantage of smoothing the gradient is that the original problem is not changed. But, we will see that more local gradients need to be evaluated in order to implement the smoothing. Therefore, the bundle method is much more expensive than the L-BFGS.

We arbitrarily choose four initial guess points from which the L-BFGS, both with and without local smoothing, failed to converge to the true solution. Figure 9 shows the performance of the bundle method for these cases chosen. It is encouraging to find that the bundle method converged to the true solution in all four cases. We then proceeded with more experiments. We repeated all the cases (a total of 49) for which either the L-BFGS without smoothing or the L-BFGS with smoothing failed. Numerical results are presented in Fig. 10. We observe that there are 18 cases where the L-BFGS method failed to find the true minimum, and 37 cases where the L-BFGS method with smoothing failed. There are six cases where both the L-BFGS without smoothing and the L-BFGS with smoothing failed. The bundle method succeeded in all 49 cases for which the L-BFGS with or without smoothing failed.

We mention, however, that there are 12 cases (out of 300 points) where the bundle method failed to find the true minimum and where the minimization using the L-BFGS method with and without smoothing was successful. This indicates that the performance of the smooth and nonsmooth optimization algorithms is case-dependent. However, we have not found a case where both the L-BFGS and the bundle method failed.

3 A discontinuous cost function using a shallow-convection observation operator

3.1 Shallow-convection

Shallow convection is sometimes called dry convection. In the 1960s, it was mainly used to allow convective adjustment in response to radiative heating so that a thermal equilibrium profile closer to the observation could be obtained (Manabe et al., 1964). In the 1980s, it began to be widely used in numerical modeling as a necessary compensation when deep convection does not occur (Betts et al., 1986).

Shallow convection is a parameterization scheme which produces a vertical thermodynamical adjustment in the atmosphere. Unlike deep convection, which has a larger vertical scale due to water vapor convergence and condensational heating, shallow convection only deals with the vertical diffusion of unstable energy. It does not involve precipitation and condensation, and its vertical scale is rather small.

The diffusion equations used in the shallow convection of the NCEP spectral model are given by

$$\frac{\partial T}{\partial t} = \frac{1}{\rho}\frac{\partial}{\partial z}\left(K_{QT}\left[\frac{\partial T}{\partial z} + \Gamma\right]\right) \tag{14}$$

$$\frac{\partial q}{\partial t} = \frac{1}{\rho}\frac{\partial}{\partial z}\left(K_{QT}\frac{\partial q}{\partial z}\right) \tag{15}$$

where T is temperature, q is specific humidity, K_{QT} is the diffusion coefficient for the temperature and humidity, and Γ is the dry adiabatic lapse rate. The discretized version of these diffusion equations forms a tridiagonal system which is solved using Gaussian elimination.

In the physical package of the NCEP global spectral model, all the unstable columns in which cumulus does not occur are picked up immediately following the Arakawa-Schubert cumulus scheme. We can summarize it in three steps:

1. Calculate the moist static energy $(gZ + C_pT + Lq)$ and identify the columns with the conditional instability $(\frac{\partial}{\partial Z}(gZ + C_pT + Lq) < 0)$. Calculate the lifting condensation level as the cloud base and the highest instability level as the cloud top. Because of vertical discretization, the cloud base/top does not change continuously when the moist static energy profile is perturbed by the change of the thermodynamical condition.

2. Assign $K_{QT} = 1.5$ m^2/s at the base; $K_{QT} = 1.0$m^2/s, at the top; $K_{QT} = 3.0$m^2/s, for the next-to-top layers; $K_{QT} = 5.0$m^2/s, for any other layers, preventing development of unrealistic kinks in the T and q profiles. The assignment of the different values of diffusion coefficient for the different cloud layer may cause discontinuities of the solution of the shallow-convection adjustment.

3. Gaussian elimination is then employed to solve the resulting tridiagonal system and the adjusted temperature and specific humidity profiles are obtained for the identified unstable columns.

The first two steps of the computational implementation of the shallow-convection parameterization may introduce discontinuities into the distribution of a cost function, defined by the shallow-convection, with respect to the model temperature and specific humidity profiles.

Figure 11 shows, for example, the distribution of the temperature adjustments at the three model levels resulting from the shallow convection with various input values of the temperature at the model level 3. The shallow-convection process is turned on and off by changing only the temperature at level 3 from $258.5K$ to $262.5K$ at an interval of $0.01K$. The adjustment occurred at three levels: levels 2, 3, and 4. It is obvious that the solution of the shallow-convection is discontinuous with respect to the input variable.

3.2 Experiment design and cost function

In order to test the performances of the L-BFGS and the nonsmooth optimization bundle algorithms using a realistic physical parameterization, the shallow-convection operator is used to define a twin experiment. The cost function is defined to measure the distance between the output of the shallow-convection operator (adjusted temperature and specific humidity profiles) and "observations" (the output temperature and specific humidity profiles for a selected input profiles of temperature and specific humidity, i.e., the true solution):

$$\begin{aligned} J_2(T,q) \;=\; & \left(\mathbf{H}_T(T,q) - T^{obs}\right)^T \mathbf{W}_T \left(\mathbf{H}_T(T,q) - T^{obs}\right) + \\ & \left(\mathbf{H}_q(T,q) - q^{obs}\right)^T \mathbf{W}_q \left(\mathbf{H}_q(T,q) - q^{obs}\right) \end{aligned} \tag{16}$$

where $\mathbf{W}_T$ and $\mathbf{W}_q$ are constant diagonal weighting matrices and their values are set to be 10^{-5} and 10^6 empirically, corresponding to typical orders of simulated temperature and specific humidity errors of 1^oC and 1 g kg^{-1}. The variables T and q in (16) are vectors of dimension K_0, which is equal to 10, the highest model level which may be affected by the shallow-convection process.

The gridded-data of temperature (T), specific humidity (q) and the surface pressure (p_s) at 00 UTC on 1 July 1995 from the NCEP re-analysis data are used for testing the performances of the L-BFGS method and the nonsmooth bundle method for minimizing J defined in (16). For a resolution of T62L28, there are a total of 47×384 columns over the entire global domain. We choose 384 columns corresponding to all the Gaussian grids around the latitude 12^o N for the test.

3.3 Performances of the L-BFGS and bundle algorithms

Among the 384 columns, there are 51 columns in which the shallow-convection process is turned on. Within these 51 columns, we selected column 111 (near 150 W) as the truth, forming the "observations" in (16). Starting from the analysis profiles at the other 383 columns, we applied both the L-BFGS and bundle algorithms to approximate the "true" atmospheric profiles of temperature and specific humidity. The L-BFGS algorithm succeeded in all 380 cases except for the three columns: 122 (at 132 W), 135 (at 107 W) and 145 (at 88 W). The bundle algorithm converged to the true solution for all 383 cases.

Tables 2-4 show the results of the minimization starting from the temperature and specific humidity profiles at the 122th, 135th, and 145th columns, respectively. Figure 12 shows the variations of the normalized cost function and the norm of the gradient (or subgradient) for the minimization starting from the temperature and specific humidity profiles at the 135th column. With six iterations the L-BFGS algorithm decreased the cost functions by about two orders of magnitude. The bundle algorithm decreased the cost functions by 3-5 orders of magnitude. The temperature and specific humidity profiles retrieved by the bundle method is much more accurate (more than an order of magnitude) than those retrieved by the L-BFGS method. The bundle method uses more function calls at each iteration than the L-BFGS method. The computational expenses of the bundle method is about twice of that of the L-BFGS method.

Table 2: Statistics on minimization of the L-BFGS and bundle methods for the example of shallow-convection with 122 column as initial guess

iteration	function calls		RMS Errors				J	
			T(^{o})		q(g/kg)			
	L-BFGS	bundle	L-BFGS	bundle	L-BFGS	bundle	L-BFGS	bundle
0	-	-	2.456	2.456	0.415	0.415	8.613	8.613
1	1	2	1.794	0.387	0.315	0.012	4.919	0.014
2	1	5	0.711	0.211	0.091	0.009	0.112	0.009
3	3	1	0.709	0.172	0.091	0.008	0.112	0.003
4	1	2	0.677	0.083	0.088	0.006	0.100	0.001
5	2	5	0.677	0.030	0.088	0.002	0.100	1.5×10^{-4}
6	2	3	0.677	0.023	0.088	0.002	0.100	0.8×10^{-4}

Figures 13-16 present the temperature and specific humidity profiles obtained at each iteration using the L-BFGS method (Figs. 13 and 15) and the bundle method (Figs. 14 and 16). We find that the adjustment made by shallow convection to the input profiles of T and

Table 3: Statistics on minimization of the L-BFGS and bundle methods for the example of shallow-convection with 135 column as initial guess

iteration	function calls		RMS Errors				J	
			T(^{o})		q(g/kg)			
	L-BFGS	bundle	L-BFGS	bundle	L-BFGS	bundle	L-BFGS	bundle
0	-	-	2.245	2.245	0.366	0.366	6.787	6.787
1	1	2	1.636	0.015	0.266	0.011	3.570	0.003
2	1	5	0.365	0.033	0.063	0.005	0.046	0.8×10^{-3}
3	4	11	0.365	0.022	0.063	0.004	0.046	0.2×10^{-3}
4	1	2	0.365	0.013	0.063	0.003	0.046	0.6×10^{-4}
5	1	2	0.365	0.009	0.063	0.002	0.046	0.2×10^{-4}
6	1	2	0.365	0.005	0.063	0.6×10^{-3}	0.046	0.4×10^{-5}

q (solid line with stars) for simulated "observations" occurred at three model levels, 3, 4 and 5, and were rather small (not shown). After the 2nd iteration, the L-BFGS minimization was stuck in a local minimum with switching turned on and off on several model levels, and had difficulty getting free and approaching the true minimum. Such a phenomenon was not seen with the bundle algorithm. Within four iterations, the minimization results approximated the true solution closely. By six iterations, differences between the minimization of the retrieved and the "observed" profiles of temperature and specific humidity were negligible. This due to the bundle algorithm property: in the first few iterations the algorithm collects information about the cost function by bundle the subgradients. After 4-5 iterations, the subgradient bundle approximates the whole generalized gradient well and the "optimal" descent direction is generated.

In order to ensure a sufficient decrease in the value of the cost function, the bundle method evaluates many sub-gradients at each iteration. For example, 10 and 19 function calls are required by L-BFGS and the bundle method to complete the six iterations, respectively. Therefore, this algorithm is much more expensive than the L-BFGS algorithm.

4 Summary and conclusions

The cost function in 4D-Var using a diabatic assimilation model with parameterized physics is only piecewise differentiable (Zhang and Zou, 1999). The differentiable minimization al-

Table 4: Statistics on minimization of the L-BFGS and bundle methods for the example of shallow-convection with 145 column as initial guess

iteration	function calls		RMS Errors				J	
			T(^{o})		q(g/kg)			
	L-BFGS	bundle	L-BFGS	bundle	L-BFGS	bundle	L-BFGS	bundle
0	-	-	2.162	2.162	0.315	0.315	4.950	4.950
1	1	2	1.402	0.317	0.215	0.010	2.268	0.012
2	1	5	0.434	0.186	0.058	0.010	0.031	0.004
3	2	3	0.413	0.139	0.057	0.007	0.029	0.001
4	2	2	0.407	0.103	0.056	0.006	0.028	0.9×10^{-3}
5	1	2	0.301	0.088	0.051	0.006	0.021	0.8×10^{-3}
6	3	4	0.292	0.077	0.050	0.005	0.019	0.6×10^{-3}

gorithms such as the limited memory quasi-Newton method that are originally designed for minimizing differentiable functions can fail. Using both a simple example and a shallow-convection scheme, we found: (i) The L-BFGS algorithm may still work well for minimizing nonsmooth cost functions. If the jumps in the cost function caused by discontinuous physics (controlled by "on-off" switches) are large, the minimization may converge to a local minimum introduced by the "on-off" switches. (ii) Introducing a weak smooth function to remove the discontinuities associated with "on-off" switches may do more damage than help to data assimilation results. The smoothing could introduce artificial stationary points, which may cause a minimization to converge to a wrong solution. (iii) The nondifferentiable bundle method performs well for minimizing nonsmooth cost functions, although it is computationally twice as expensive as the L-BFGS method. Although a strong smoothing does not cause problem for the differentiable minimization to converge and may be applied, the consequence of such a strong smoothing on changing the prediction of atmospheric state needs to be studied beforehand.

We have used simple models for examining the performance of differentiable and nondifferentiable optimization algorithms for discontinuous cost functions. We plan to test the feasibility of applying the nondifferentiable minimization algorithm, such as the bundle method (Lemaréchal 1989), to 4D-Var using the NCEP adiabatic model and comparing the accuracy of the solution with that using the differentiable minimization methods.

Acknowledgements

This research is supported by NOAA grant NA37WA0361 and NSF grant ATM-9812729. The authors would like to thank Dr. E. Kalnay for her persistent encouragement on this study. We also thank Dr. Claude Lemaréchal from I.N.R.I.A. for providing to us the software for his bundle method. The original bundle algorithm was modified by Profs. Navon and Nazareth to fit the test problems.

REFERENCES

Arakawa, A. and W. H. Schubert, 1974: Interaction of a cumulus ensemble with the large-scale environment, Part I. *J. Atmos. Sci.,* **31**, 674–701.

Betts, A. K., 1986: A new convective adjustment scheme. Part I: Observational and theoretical basis. *Quart. J. Roy. Meteor. Soc.,* **112**, 677–691.

Broyden, C. G., 1970: The convergence of a class of double rank minimization algorithms. Parts I and II. *J. Inst. Maths. Applics.***6**, 76–90.

Fletcher, R., 1970: A new approach to variable metric algorithms. *Computer Journal,***13(3)**, 312–322.

Ghil, M., S. Cohn, J. Tavantzis, K. Bube and E. Isaacson, 1981: Applications of estimation theory to numerical weather prediction, in Dynamical meteorology. Data assimilation methods. New York, 139–224.

Goldfarb, D., 1970: A family of variable metric methods derived by variational means. *Math. of Comp.***24**, 23–26.

Hiriart-Urruty, J-B and C. Lemaréchal, 1993: Convex analysis and minimization algorithms II: Advanced theory and bundle methods. Springer-Verlag, Vol. 306, 346pp

Hong, S. Y. and H. L. Pan, 1996: Nonlocal boundary-layer vertical diffusion in a medium-range model. *Mon. Wea. Rev.,* **124**, 2322–2339.

Kanamitsu M., J.C. Alpert, K.A. Campana, P.M. Caplan, D.G. Deaven, M. Iredell, B. Katz, H.-L. Pan, J. Sela and G.H. White, 1991: Recent changes implemented into global forecast system at NMC. *Weather and Forecasting* **6**, 425–435.

Kiwiel, K.C., 1985: Methods of descent for nondifferentiable optimization. Springer-Verlag, Lecture notes in mathematics, Vol. 1133, 362pp

Kuo, Y.-H., X. Zou and Y.-R. Guo, 1996: Variational assimilation of precipitable water using a nonhydrostatic mesoscale adjoint model. Part I: Moisture retrieval and sensitivity experiments. *Mon. Wea. Rev.,* **124**, 122–147.

Le Dimet, F. X. and O. Talagrand, 1986: Variational algorithms for analysis and assimilation of Meteorological observations: Theoretical aspects. *Tellus,* **38A**, 97–110.

Leith, C.E., 1971: Atmospheric predictability and two-dimensional turbulence. *J. Atmos. Sci.,* **28**, 145–161.

Lemaréchal, C., 1977: Bundle methods in nonsmooth optimization. Proceeding IIASA series. by C. Lemaréchal and R. Mifflin, Eds, Pergamon press, 186pp, 79–103

Lemaréchal, C., 1978: Nonsmooth optimization and descent methods. International Institute for Appl. Sys. Analysis, Laxenburg, Austria, 25pp

Lemaréchal, C., 1989: Nondifferentiable optimization. *Optimization*, *Handbooks in OR&MS*, **1**, G. L. Nemhauser et al. (eds.), Elsevier Science Publishers, 529–572.

Lemaréchal, C. and C. Sagastizabal 1997: Variable metric bundle methods: From conceptual to implementable forms. *Mathematical Programming*, **76**, 393–410.

Liu, D. C., and J. Nocedal, 1989: On the limited memory BFGS method for large scale optimization. *Mathematical Programming* , **45**, 503-528.

Manabe, S. and R. F. Strickler, 1964: Thermal equilibrium of the atmosphere with a convection adjustment. *J. Atmos. Sci.,* **21**, 361–385.

Navon, I. M., X. Zou, J. Derber, and J. Sela, 1992: Variational data assimilation with an adiabatic version of the NMC spectral model. *Mon. Wea. Rev.,* **120**, 1433-1446.

Nocedal J,1980: Updating Quasi-Newton Matrices with Limited Storage, *Mathematics of Computation***35**, 773–782.

Pan, H. L. and W. S. Wu, 1995: Implementing a mass flux convection parameterization package for the NMC medium-range forecast model. *Techical Report for NMC/NOAA/NWS*, No. **409**.

Pierrehumbert, R. T., 1986: An essay on the parameterization of orographic gravity wave drag. *GFDI/NOAA*, Princeton University, Princeton, NJ08542.

Poljak, B. T., 1977: Subgradient methods: A survey of Soviet research in nonsmooth optimization. C. Lemaréchal and R. Miff Liu, Eds, Pergamonn press, 5-31,186pp

Rabier F., J.-N. Thepaut and P. Courtier, 1998: Extended assimilation and forecast experiments with a four-dimensional variational assimilation system. *Quart. J. Roy. Meteor. Soc.,* **124**, 1861–1887.

Sela, J., 1982: The NMC spectral model. *NOAA technical report, NWS 30, NWS/NOAA, US Department of Commerce*, 36pp.

Sela, J., 1987: The new T80 NMC operational spectral model. *Preprint, the Eighth conference on Numerical Weather Prediction, Baltimore, Maryland, February 22-26,1988.*

Shanno, D. F., 1970: Conditioning of quasi-Newton methods for function minimization. *Math. of Comp.***24**, 647–657.

Shor, N. Z., 1985: Minimization methods for nondifferentiable functions. Springer-Verlag (translated from Russian, 1979 by K.C. Kiwiel and A. Ruszczynski), 162pp

Thepaut, J. N. and P. Courtier, 1991: 4-dimensional data assimilation using the adjoint of a multilevel primitive equation model. *Quart. J. Roy. Meteor. Soc.,* **117**, 1225–1254.

Tsuyuki, T., 1997: Variational data assimilation in the tropics using precipitation data. Part III: Assimilation of SSM/I precipitation rates. *Mon. Wea. Rev.,* **125**, 1447–1464.

Xiao Q., and X. Zou, and Y.-H. Kuo, 1999: Incorporating the SSM/I derived precipitable water vapor and rain rate into a numerical model: A Case study for ERICA IOP-4 cyclone. *Mon. Wea. Rev.*, (in press).

Zhang, S. and X. Zou, 1999: Further discussions on the use of adjoint of discontinuous model physics in 4D-Var. *Submitted to* **Tellus**.

Zou, X., 1997: Tangent linear and adjoint of "on-off" processes and their feasibility for use in 4-dimensional variational data assimilation. *Tellus,* **49A**, 3–31.

Zou, X., I. M. Navon, M. Berger, Paul K. H. Phua, T. Schlick, and F. X. LeDimet, 1993: Numerical experience with limited-memory quasi-Newton and truncated-Newton methods. *SIAM Journal on Optimization*, **3**, 582-608.

Zou, X., and Y.-H. Kuo, 1996: Rainfall assimilation through an optimal control of initial and boundary conditions in a limited-area mesoscale model. *Mon. Wea. Rev.,* **124**, 2859-2882.

Zou, X., H. Liu, J. Derber, J. G. Sela, R. Treaton, and B. Wang, 1999: Four-dimensional variational data assimilation with a full-physics version of the NCEP spectral model: System development and preliminary results. (submitted to Quart. J. Roy. Meteor. Soc.)

Zupanski, D., 1993: The effects of discontinuities in the Betts-Miller cumulus convection scheme on four-dimensional variational data assimilation in a quasi-operational forecasting environment. *Tellus,* **45A**, 511–524.

Zupanski, D. and F. Mesinger, 1995: Four-dimensional variational assimilation of precipitation data. *Mon. Wea. Rev.,* **123**, 1112–1127.

FIGURE CAPTIONS

Fig. 1 The performances of the L-BFGS algorithm for minimizing the cost function J_1 defined in (2) through (3), a piecewise differentiable cost function, starting from different initial guess points: a) $x_0 = 2$, b) $x_0 = 2.29$, c) $x_0 = 2.80$ and c) $x_0 = 2.90$. The time window includes 4-step time steps, i.e., $t_R = t_0 + 4\Delta t$, $\Delta t = 0.1$. The cost function (solid curve) is obtained by evaluating the function at the different initial conditions with an interval of 0.01. The numbers in the figures are the iteration numbers and the black dots represent the value of J obtained at each iteration.

Fig. 2 Same as Fig. 1 except for the minimization starting from the initial guess point $x_0 = 2.55$.

Fig. 3 The Distributions of the cost function J_1 defined in (2) through (1) with $f_1 = 2x - 2$ and $f_2(x) = x - 4$ (thin solid line), $f_2(x) = x - 3.5$ (thick dotted line) and $f_2(x) = x - 3$ (thick solid line).

Fig. 4 Distributions of the model forcing $f(x)$ (see 6) with (dotted line) and without (solid line) smoothing when h=0.1 and $\alpha = 100$.

Fig. 5 Distributions of (a) the cost function and (b) the gradient with (dotted lines for h=0.1 and $\alpha = 100$) and without (dotted lines) smoothing.

Fig. 6 Same as Fig. 4 except for $h = 0.2$, $alpha = 20$ (thick dashed line) and $h = 0.5$, $alpha = 5$ (thick dotted-dashed line).

Fig. 7 Same as Fig. 5 except for $h = 0.2$, $alpha = 20$ (thick dashed line) and $h = 0.5$, $alpha = 5$ (thick dotted-dashed line).

Fig. 8 Same as Fig. 1 except that the local smoothing (see 6) is introduced at the switching point. A "2..." indicates the minimization process is stuck around the same point after 2 iterations.

Fig. 9 Same as Fig. 1 except that the nondifferentiable bundle algorithm is used and the initial guess values of (a) $x_0 = 2.54$, b) $x_0 = 2.57$, c) $x_0 = 2.92$ and d) $x_0 = 2.95$ are used. The L-BFGS with and without smoothing failed in all these four cases.

Fig. 10 The solutions obtained by the L-BFGS method with (diamonds connected by dotted line) and without (dots connected by thin solid line) and the bundle method (thick solid line) for the 49 cases for which the L-BFGS method with or without smoothing failed.

Fig. 11 Distributions of the temperature adjustments at model level 2 (solid line), 3 (dotted line) and 4 (dashed line) due to shallow convection for various values of the input temperature at the model level 3. The temperature interval for the input temperature at the model level 3 at which these calculations are made is 0.01^oC.

Fig. 12 The logarithmic variations of the normalized values of the cost function (solid lines) and the gradient (dashed lines) with the number of iterations using the L-BFGS (thin solid and dotted lines) and the bundle (thick solid and dotted lines). The cost function is defined by (16) using shallow convection.

Fig. 13 The temperature profiles before and after the shallow-convection adjustments at (a) the 0th and the first iteration, (b) the second iteration, (c) the third iteration, and (d) the fourth iteration using the L-BFGS method. The true temperature profiles, i.e., the profile which was used to generate "observations" using shallow convection, is presented in each panel (solid lines with stars).

Fig. 14 Same as Fig. 11 except using the nondifferentiable bundle method.

Fig. 15 Same as Fig. 11 except for the specific humidity variable.

Fig. 16 Same as Fig. 12 except for the specific humidity variable.

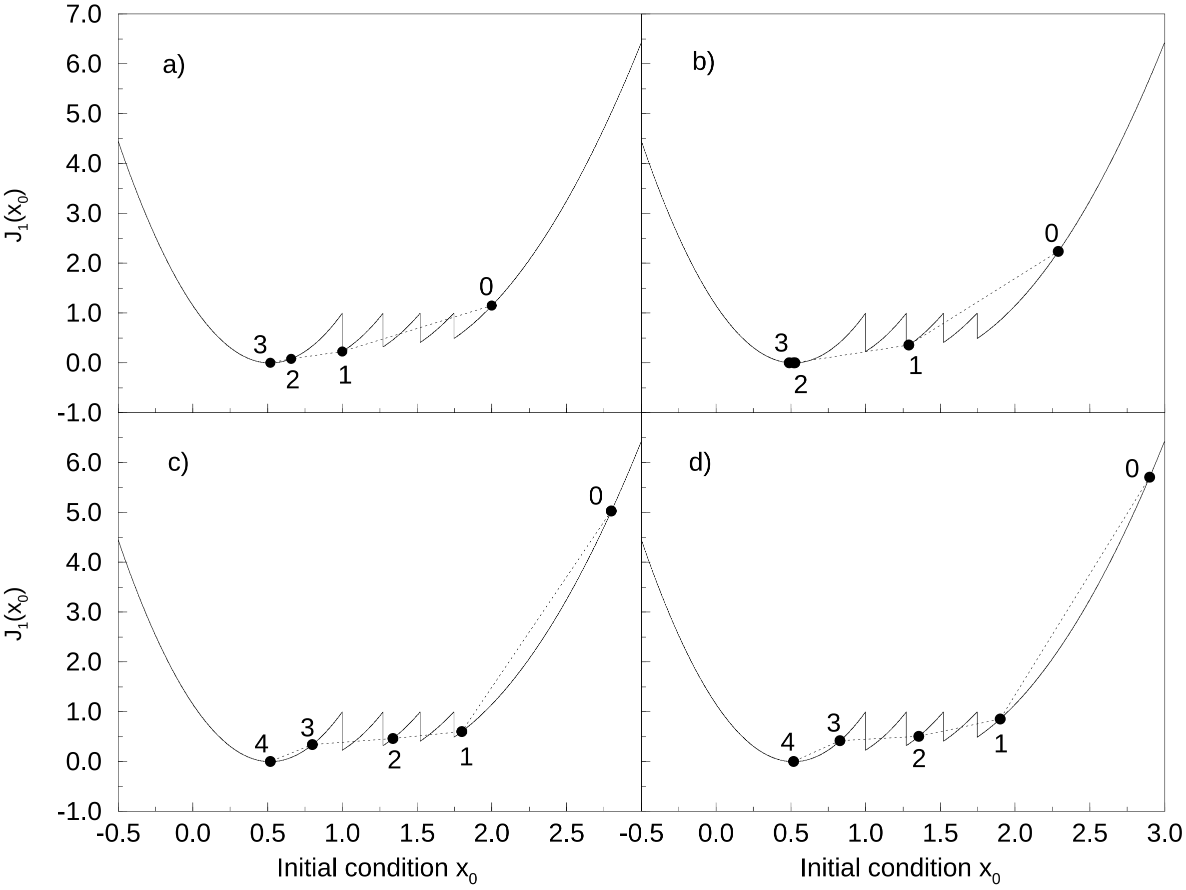

a)
b)
c)
d)
$J_1(x_0)$
$J_1(x_0)$
Initial condition x_0
Initial condition x_0
7.0
6.0
5.0
4.0
3.0
2.0
1.0
0.0
-1.0
-0.5
0.0
0.5
1.0
1.5
2.0
2.5
3.0

Figure 1:

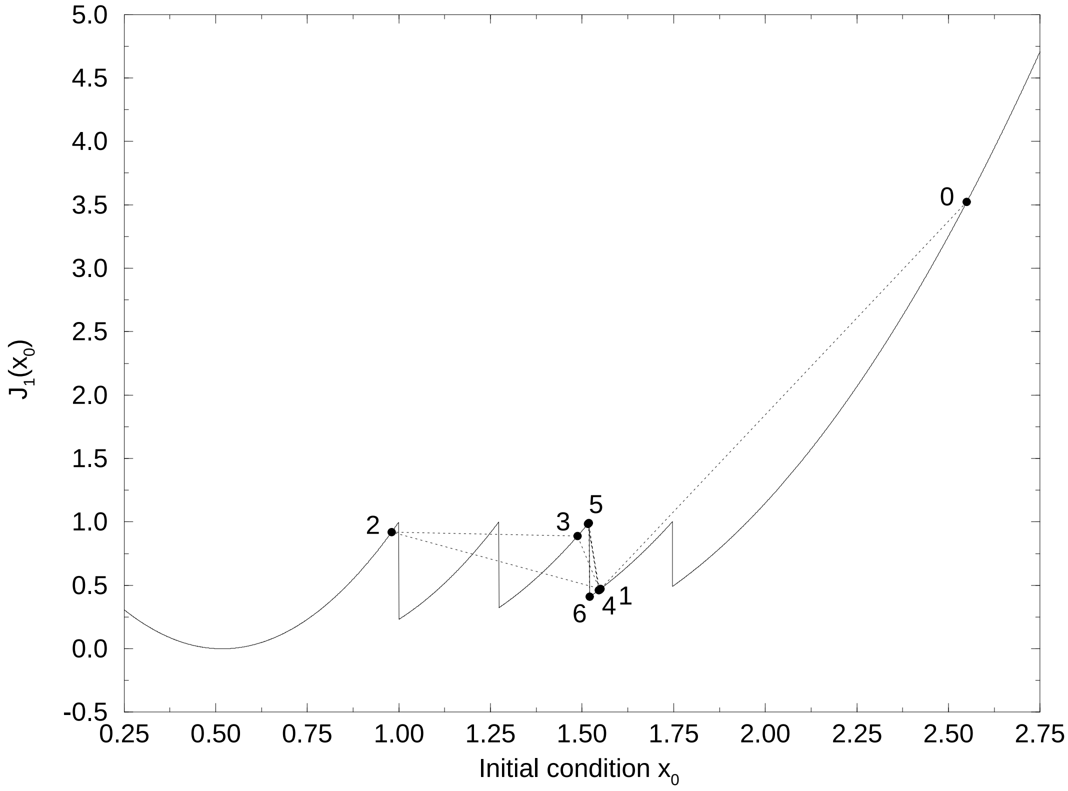

5.0
4.5
4.0
3.5
3.0
2.5
2.0
1.5
1.0
0.5
0.0
-0.5
0.25
0.50
0.75
1.00
1.25
1.50
1.75
2.00
2.25
2.50
2.75
$J_1(x_0)$
Initial condition x_0
0
1
2
3
4
5
6

Figure 2:

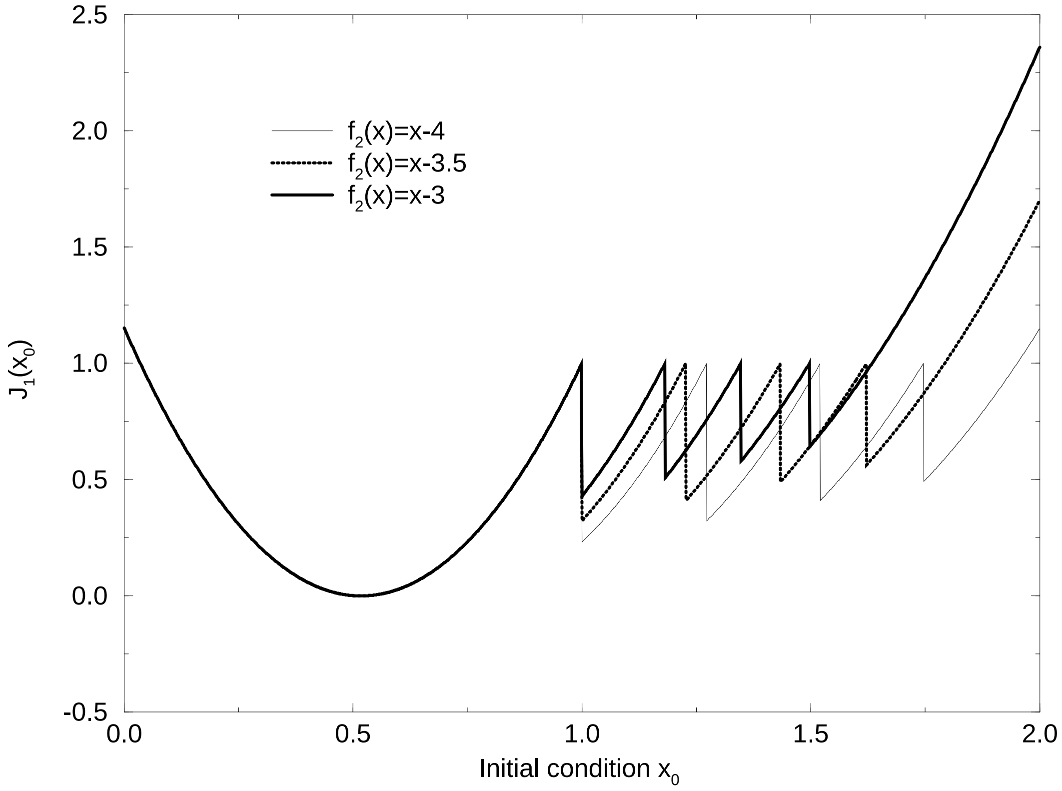

2.5
2.0
1.5
1.0
0.5
0.0
-0.5
0.0
0.5
1.0
1.5
2.0
$J_1(x_0)$
Initial condition x_0
$f_2(x)$=x-4
$f_2(x)$=x-3.5
$f_2(x)$=x-3

Figure 3:

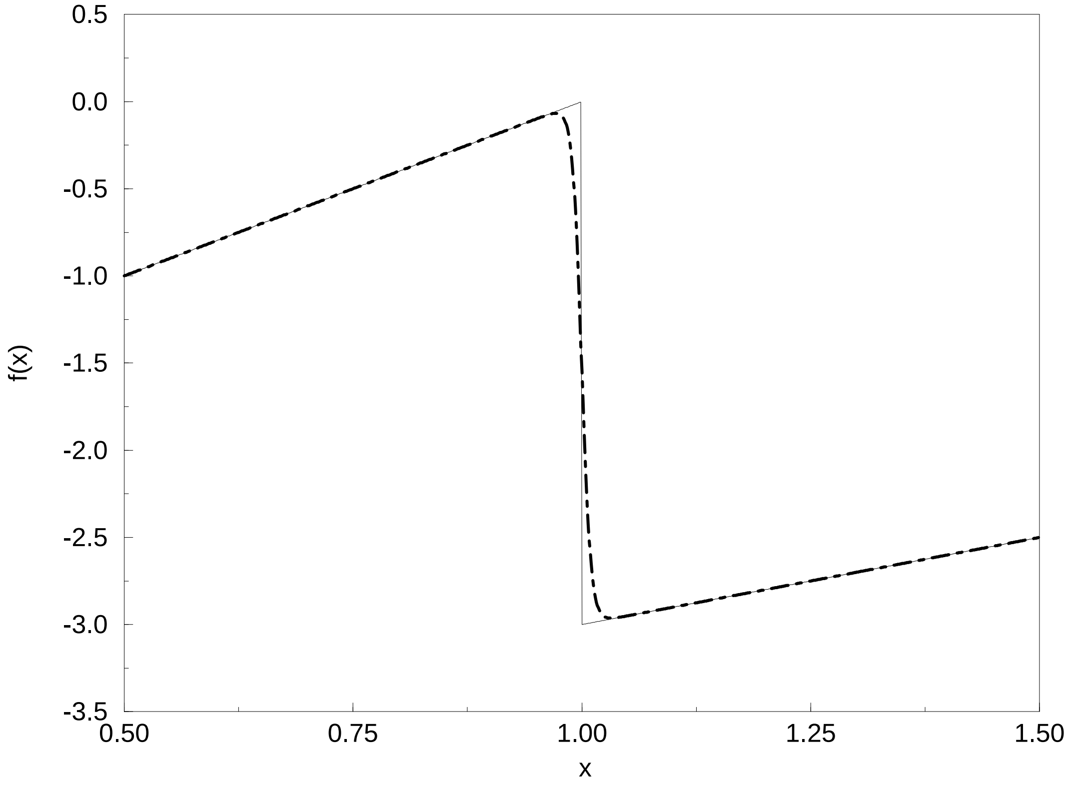

Figure 4:

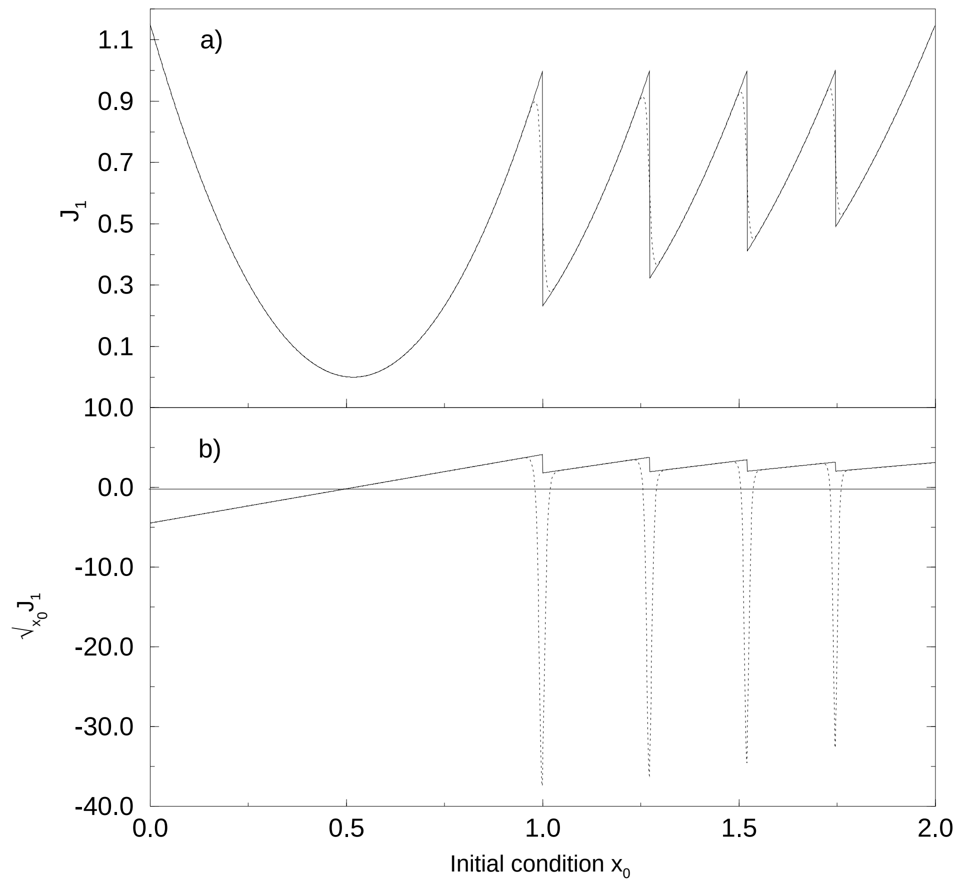

a)
1.1
0.9
0.7
0.5
0.3
0.1
J_1
b)
10.0
0.0
-10.0
-20.0
-30.0
-40.0
$\nabla_{x_0} J_1$
0.0
0.5
1.0
1.5
2.0
Initial condition x_0

Figure 5:

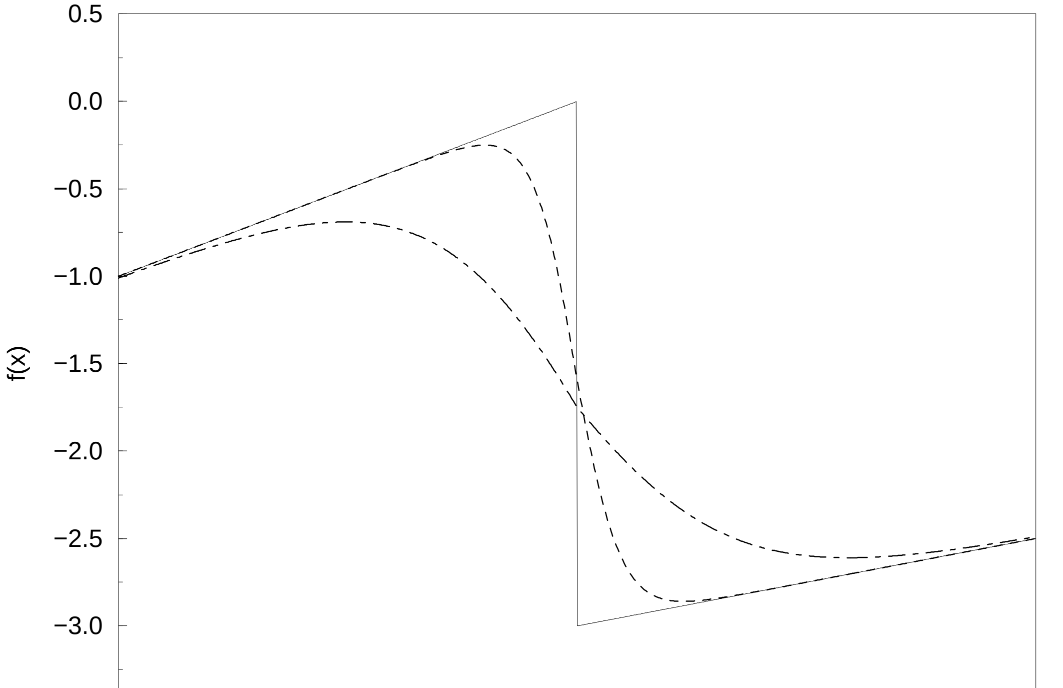

Figure 6:

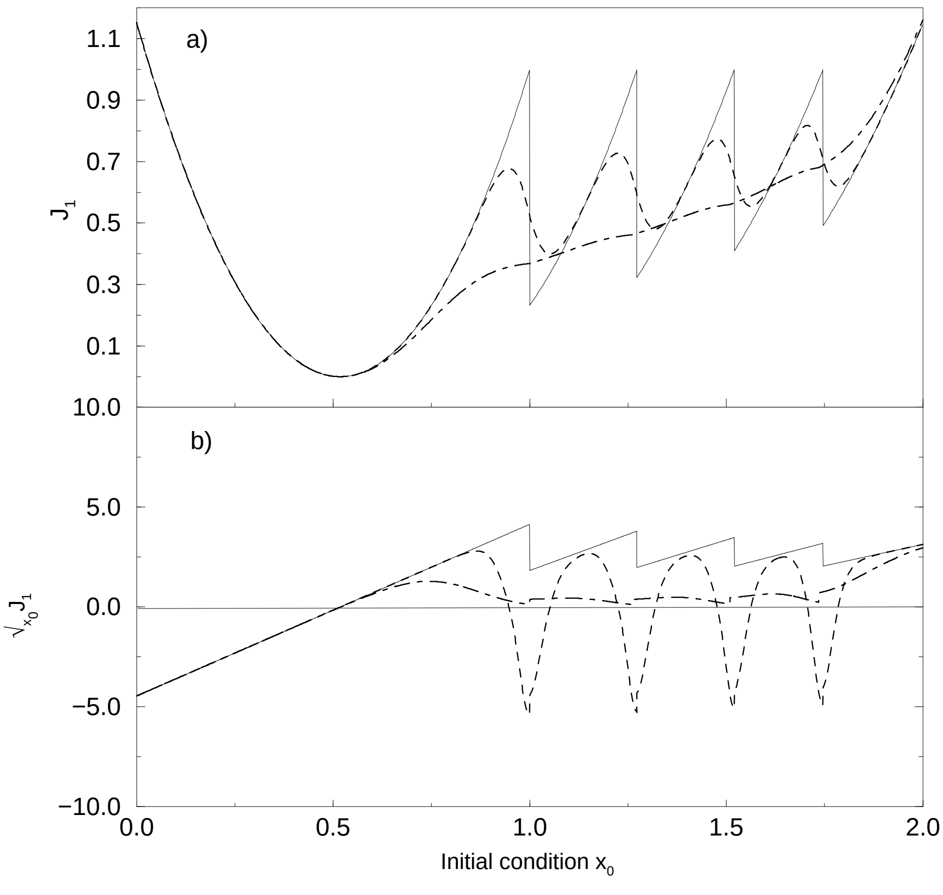
a)
b)
1.1
0.9
0.7
0.5
0.3
0.1
10.0
5.0
0.0
−5.0
−10.0
J_1
$\surd_{x_0} J_1$
0.0
0.5
1.0
1.5
2.0
Initial condition x_0

Figure 7:

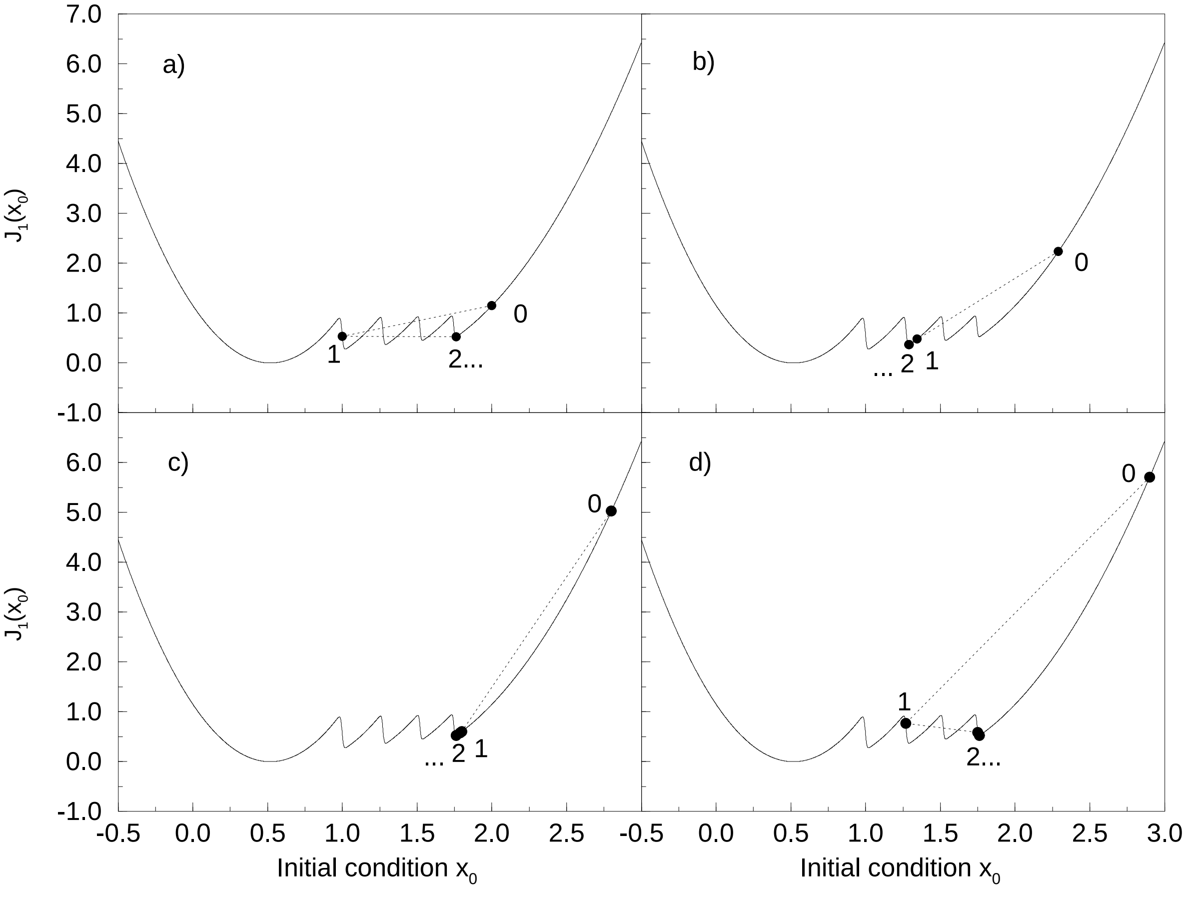

a)
b)
c)
d)
0
1
2...
... 2
1
J$_1$(x$_0$)
Initial condition x$_0$
7.0
6.0
5.0
4.0
3.0
2.0
1.0
0.0
-1.0
-0.5
0.0
0.5
1.0
1.5
2.0
2.5
3.0

Figure 8:

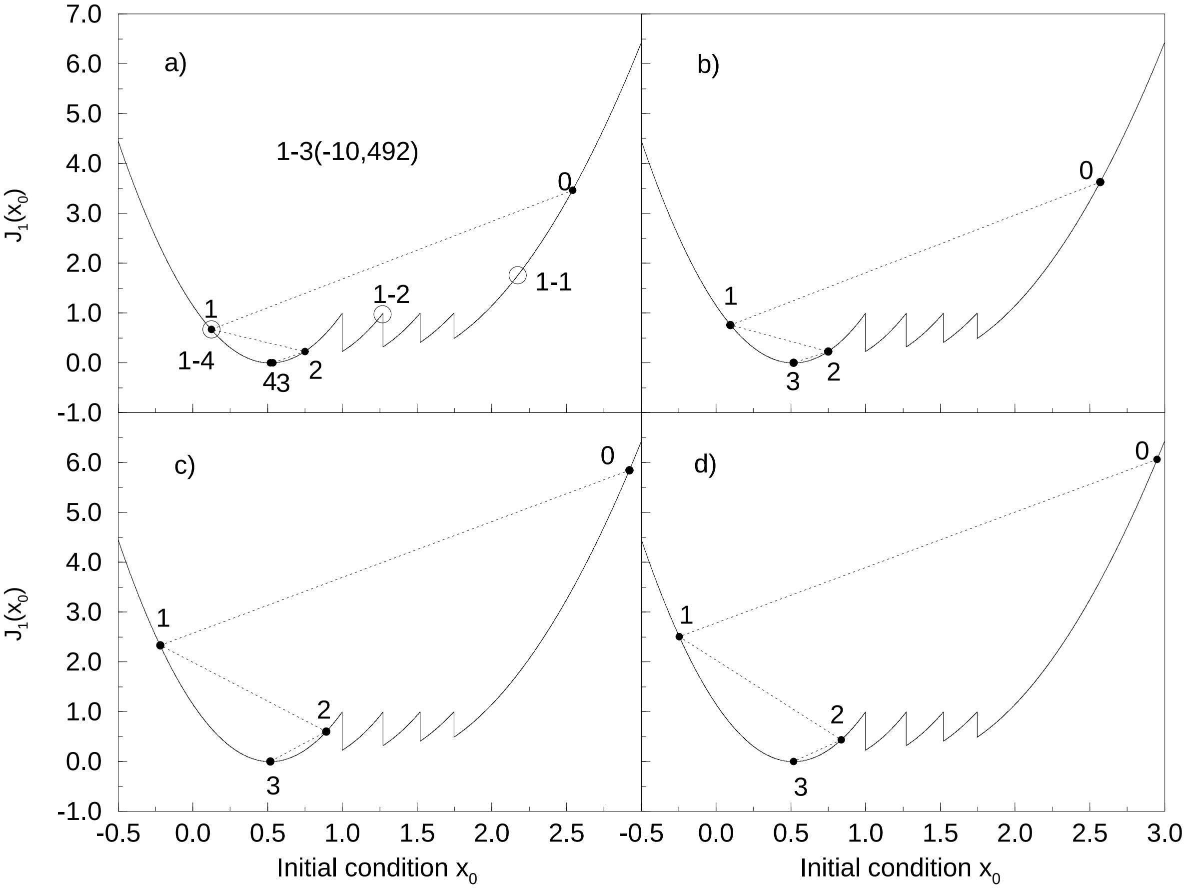
a)
b)
c)
d)
1-3(-10,492)
0
1
2
3
4
1-1
1-2
1-4
$J_1(x_0)$
Initial condition x_0
7.0
6.0
5.0
4.0
3.0
2.0
1.0
0.0
-1.0
-0.5
0.0
0.5
1.0
1.5
2.0
2.5
3.0

Figure 9:

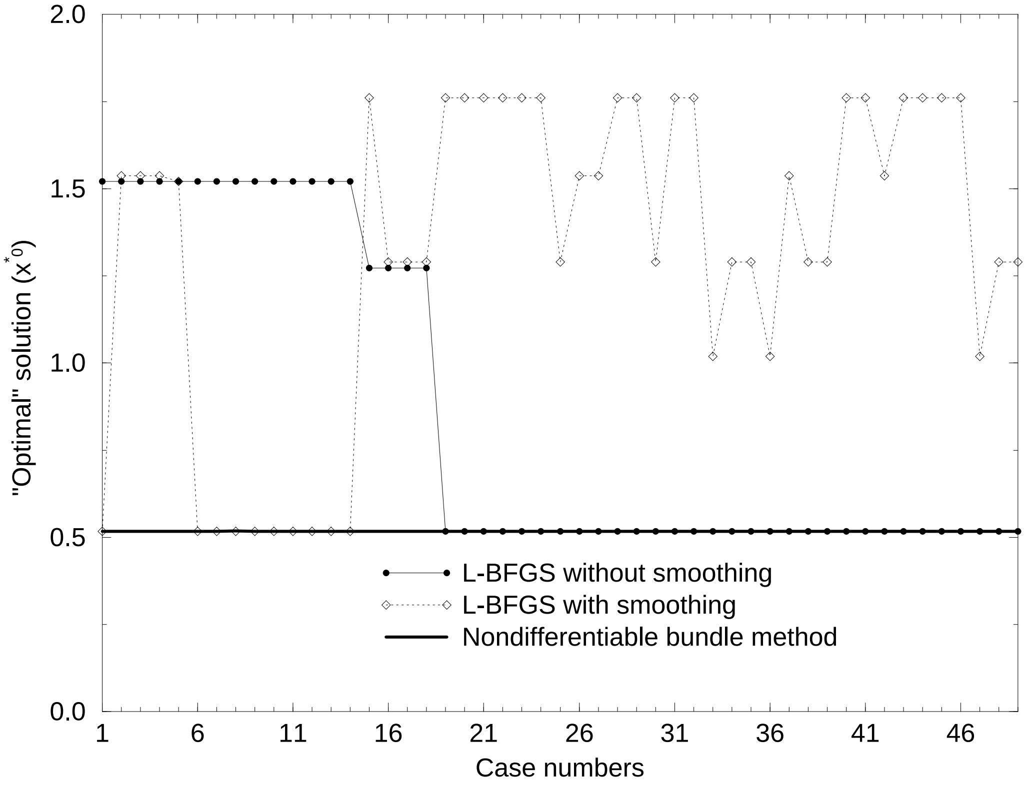

2.0
1.5
1.0
0.5
0.0
"Optimal" solution (x^{*0})
1
6
11
16
21
26
31
36
41
46
Case numbers
L-BFGS without smoothing
L-BFGS with smoothing
Nondifferentiable bundle method

Figure 10:

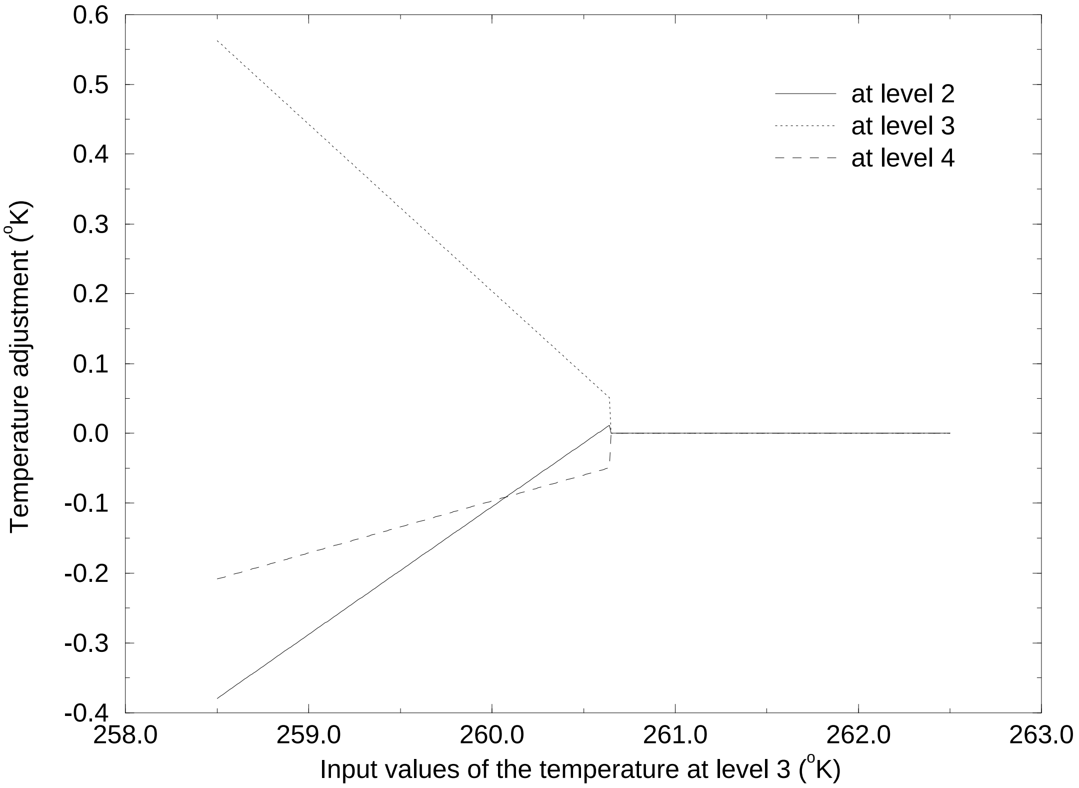
0.6
0.5
0.4
0.3
0.2
0.1
0.0
-0.1
-0.2
-0.3
-0.4
Temperature adjustment (oK)
at level 2
at level 3
at level 4
258.0
259.0
260.0
261.0
262.0
263.0
Input values of the temperature at level 3 (oK)

Figure 11:

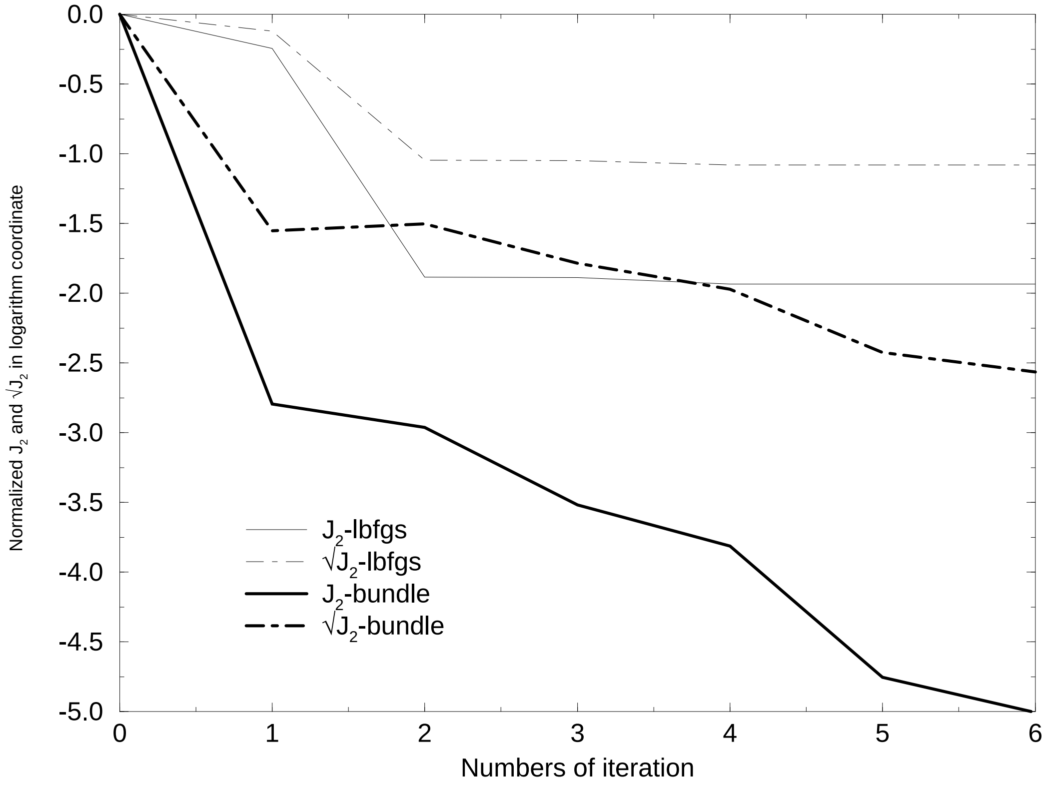
0.0
-0.5
-1.0
-1.5
-2.0
-2.5
-3.0
-3.5
-4.0
-4.5
-5.0
0
1
2
3
4
5
6
Normalized J2 and √J2 in logarithm coordinate
Numbers of iteration
J2-lbfgs
√J2-lbfgs
J2-bundle
√J2-bundle

Figure 12:

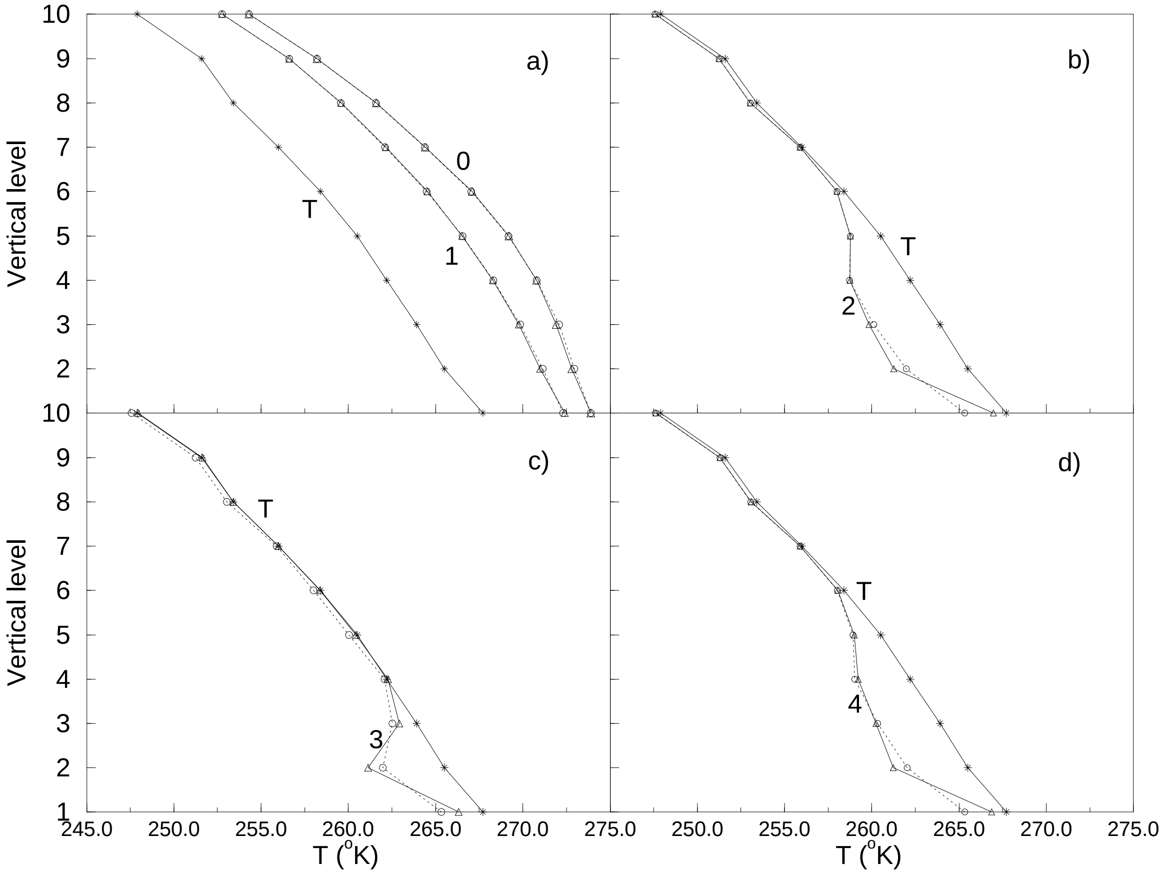
a)
b)
c)
d)
Vertical level
Vertical level
T (^{o}K)
T (^{o}K)
T
0
1
2
3
4
245.0
250.0
255.0
260.0
265.0
270.0
275.0

Figure 13:

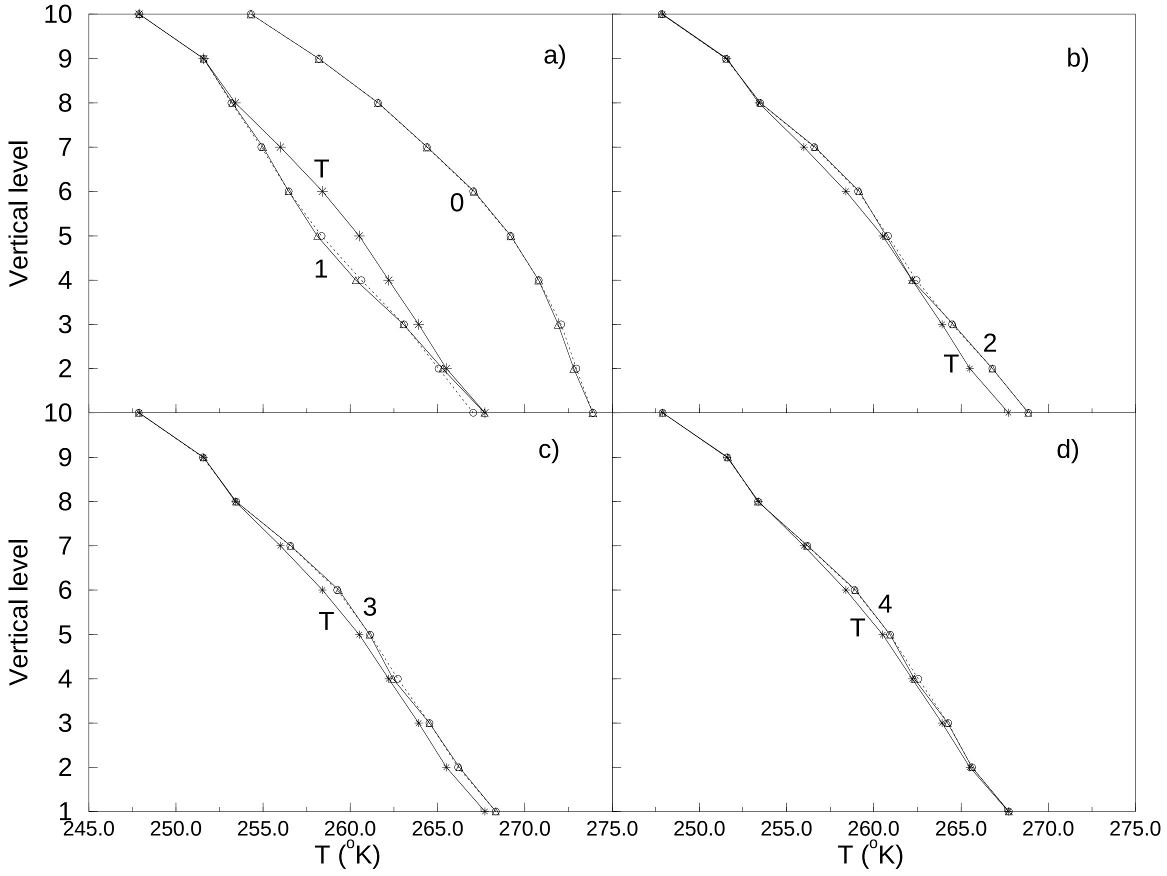
a)
b)
c)
d)
T
0
1
2
3
4
Vertical level
T (oK)
245.0
250.0
255.0
260.0
265.0
270.0
275.0

Figure 14:

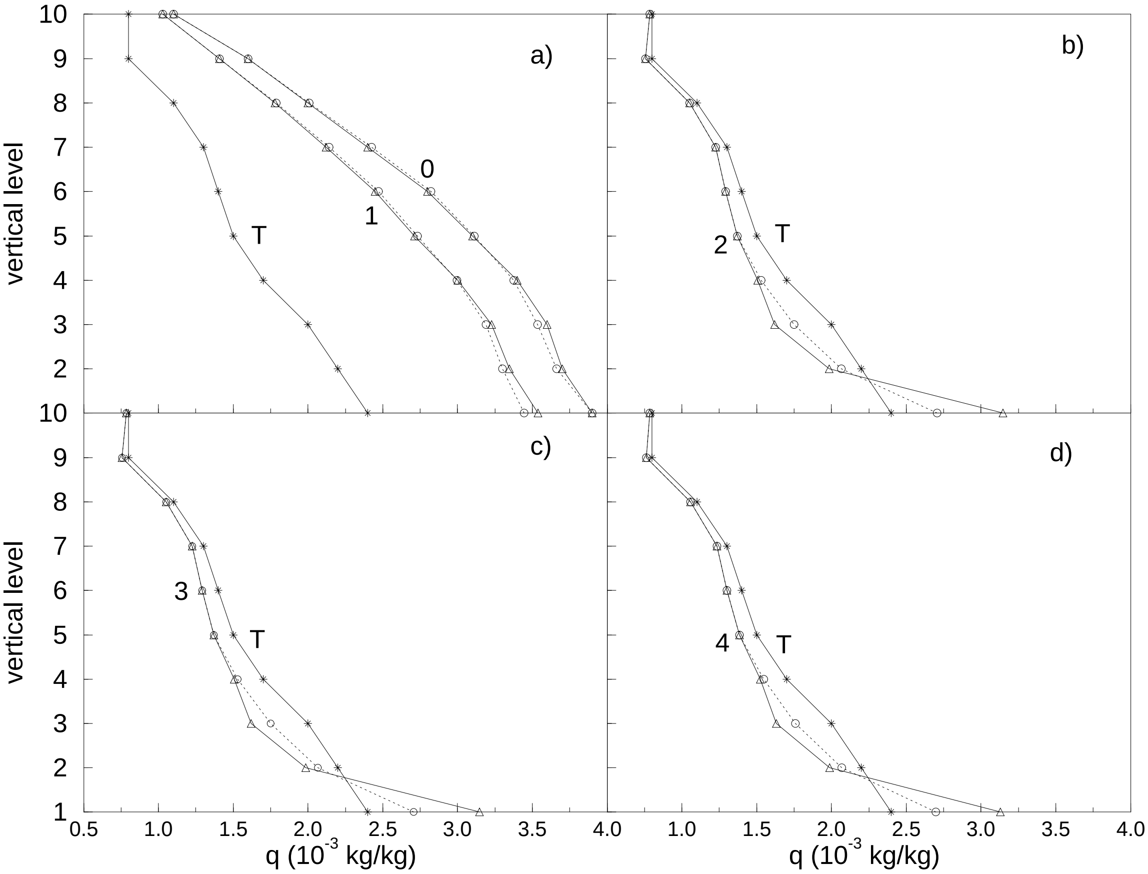

a)
b)
c)
d)
0
1
2
3
4
T
T
T
T
vertical level
vertical level
q (10^-3 kg/kg)
q (10^-3 kg/kg)

Figure 15:

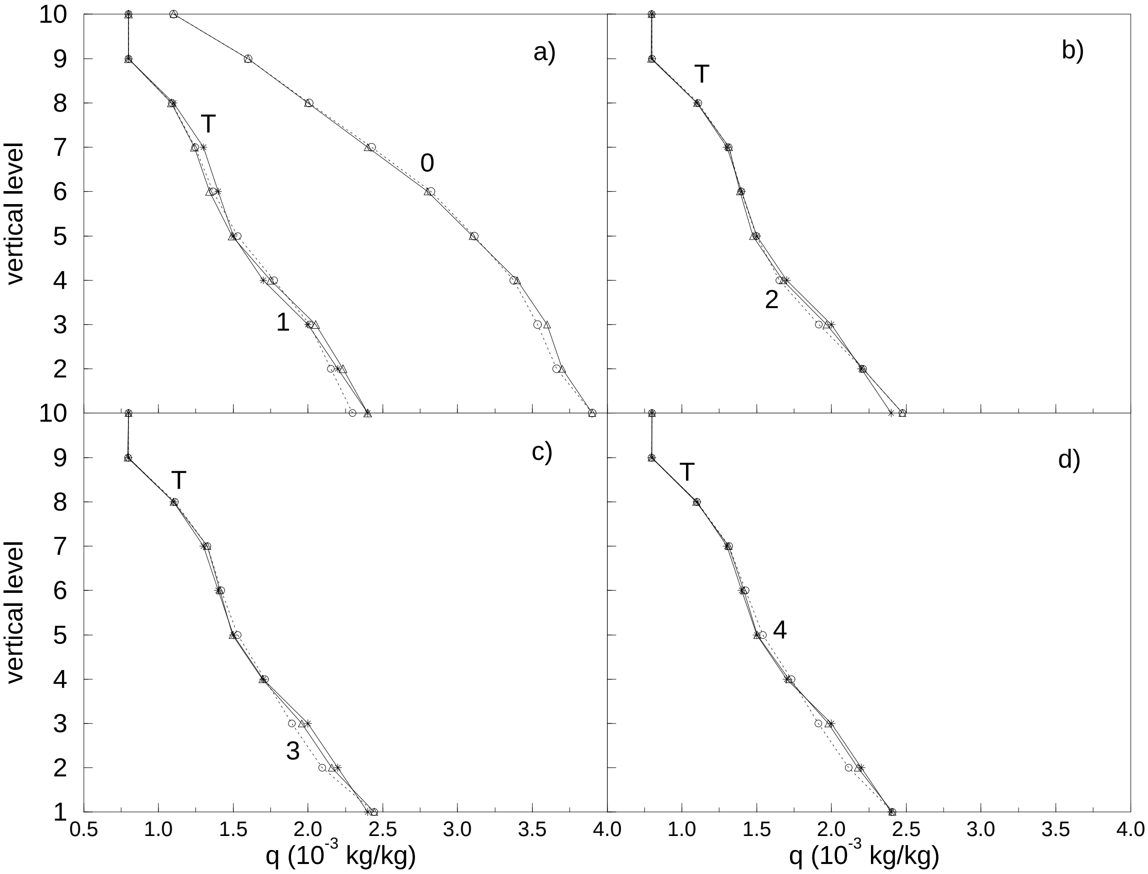

Figure 16: